Effect of nickel substitution on structural, optical and dielectric properties of lead chalcogenide (PbSe) nano particle

N. PRIYADHARSINI[a], M. THAMILSELVAN[a,*], S. VAIRAM[b]
Department of Physics, Thanthai Periyar Government institute of technology, Vellore, India
Department of Chemistry, Government college of technology, Coimbatore, India

Nickel doped PbSe ($Pb_{1-x}Ni_xSe$) nanoparticles was successfully synthesized through the wet chemical method at room temperature. Structural, composition and morphology of the as-obtained samples were characterized by X-ray diffraction (XRD), scanning electron microscopy (SEM), energy-dispersive X-ray spectroscopy (EDX) and transmission electron microscopy (TEM). The XRD pattern recorded for the $Pb_{1-x}Ni_xSe$ nanoparticles confirms the cubic structure and particle size increases as nickel content increase. The SEM images show the dense microstructure for pure PbSe and well defined particles for nickel substituted PbSe. EDX confirmed the purity of the as-obtained powders. The SAED patterns predicted crystalline nature and particle size was found in the range of 20-35 nm through TEM analysis. The studies on the optical property of $Pb_{1-x}Ni_xSe$ were carried out by UV-vis absorption spectrum; it shows the direct transition and the band gap value decrease with increasing Ni content in lead chalcogenide. The strong influence of the nickel (dopant) substitution on dielectric analysis of the samples was witnessed from the electrical measurements.

1. Introduction

In recent years, there has been a considerable interest in chalcogenide semiconductors due to their remarkable optical and electrical properties. Among these, PbSe is an inspiring material due to its narrow band gap (0.27 eV) with high carrier mobility, positive temperature coefficient of resistance and strong ionic character compared with other lead chalcogenides such as PbS, PbTe [1-4]. PbSe has unique physical properties such as optical, electrical and magnetic properties, and it has an important application in infrared detectors, sensors, photocatalytics, thermoelectricity and solar cell panels [5-7]. The high permittivity of lead chalcogenides can effectively shield the charge carriers from the lattice defects, yielding superior fault-tolerant properties [8]. PbSe and their alloys have a technical importance in the form of crystalline and polycrystalline, as photoresistors, lasers, optoelectronic devices, infrared emitters and solar control coatings [9-11]. Polycrystalline semiconductor (PbSe) has much interest in an expanding variety of applications in electronic and optoelectronic devices. Due to its extensive applications, lead chalcogenide semiconductors received enormous attention by many research groups.

Molecular beam epitaxy, sonochemical, photochemical, solvothermal, hydrothermal, colloidal synthesis, wet chemical protocol and electro-deposition methods have been employed for the fabrication of PbSe nanoparticles with various morphologies such as nanorings, nanocubes, nanorods and nanotubes [12-15].

Among these various synthesis methods, wet chemical protocol method is a single step, direct synthesis route, which has many advantages such as precise size control, homogeneous state at a molecular level cost effective, more versatile, and desirable morphology of the product.

Doping is an important parameter to improve the physical properties of semiconductors and the results are in the range of remarkable effects comparing with undoped material [16]. In this work, the structural and optical properties of wet chemical synthesis of nickel doped and undoped lead selenide nanoparticles have been analyzed. The crystal structure and band gap of $Pb_{1-x}Ni_xSe$ can be tailored by changing the concentration of nickel. For maximum efficiency of electrical energy, one can suitably tune the visible region of the electromagnetic spectrum. In view of low production cost and the extensive applications of polycrystalline lead chalcogenides in infrared optoelectronics, this preparation method can be used in future.

2. Experimental procedure

Nickel doped lead selenide ($Pb_{1-x}Ni_xSe$; x=0, 0.05, 0.10 and 0.15) nanoparticles were prepared by wet chemical precipitation method. Lead nitrate ($PbNO_3$), nickel acetate hexahydrate (Ni $(CH_3COO)_2.6H_2O$ and selenium dioxide (SeO_2) were purchased from Merck and dissolved using millipore water for required ratios. Hydrazine hydrate was added as precipitant and used as a

reducing agent in the experiment. Initially, 2g of Lead nitrate and stoichiometrically measured nickel acetate hexahydrate (dopant) precursors were added together and stirred for an hour to attain the turbid free clear solution. The precipitation process was carried by drop wise addition of selenium dioxide in the above mixture under vigorous stirring, followed by addition of hydrazine hydrate and fixes the pH 9.0. As soon as the hydrazine hydrate is added, the turbid solution is turned into flesh pink precipitate and the same is allowed to stir for 12 hrs for ageing. The resultant product was centrifuged, washed thoroughly with acetone and the samples were dried at room temperature.

2.1. Characterization technique

The samples were subjected to analytical measurements for material confirmation and evaluation of physical properties. X-ray measurement of samples was done by using XPERT-PRO diffractometer at the scanning rate of 0.02°/min for the range from 10° –80° using Cu-K$_\alpha$ source. Scanning Electron Micrographs (SEM) recorded on SEMJEOL JAX-840A electron micro analyzer which was also equipped with Energy Dispersive X-ray (EDAX) photometer. Further, to study the highly resolved microstructure and morphology, the samples were subjected to Transmission Electron Microscope (TEM) using PHILIPS CM200, with operating voltages 20-200 KV. Optical properties of the samples were evaluated by UV-VIS spectroscopy using JASCO V-570 Spectrophotometer ranging from 200 nm to 2000 nm at the slit width of 1 nm. The dielectric analysis was performed by pelletizing the nanopowders and were given the ohmic contact and measure using PRECISION IMPEDANCE ANALYZER 6000B (LCR-Z meter) for the frequency range 100 KHz to 5 MHz at room temperature.

3. Results and discussions

3.1. Structural analysis

X-ray diffraction patterns for different dopant concentration of nickel in $Pb_{1-x}Ni_xSe$ (x= 0, 0.05, 0.10, 0.15) samples at pH 9.0 are shown in Fig. 1. All peaks obtained are characteristics of cubic structure with preferential orientation along (1 1 1), (2 0 0), (2 2 0), (3 1 1), (2 2 2) and (4 0 0) planes with Fm3m space group. The peaks are well indexed with JCPDS and no other secondary phases are detected (PDF# 78-1903; ICSD# 06-3097). The width of peak confirms nano size particles and the intensity of peak indicates the improved crystalline nature.
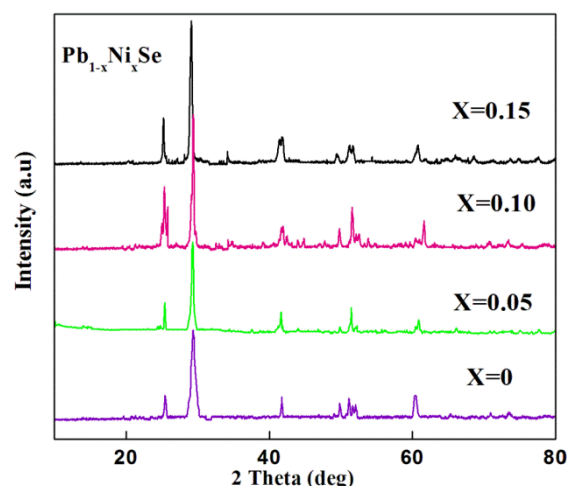
Fig. 1. XRD spectra of pure and nickel doped PbSe nanoparticles at pH 9.0

The predominant (2 0 0) peak is observed in all samples, whose intensity is enhanced with increasing nickel content. Diffraction intensity of preferential orientation peak is the accumulative effect of all equivalent crystal planes in X-ray diffraction pattern is called multiplicity factor [17, 18]. The full width half maximum (FWHM, β) value decreases with dopant concentration. The crystalline size was calculated using Debye- Scherer formula [19],

$$D = \frac{0.9\,\lambda}{\beta\cos\theta} \qquad (1)$$

Where β is the full width half maximum of diffraction peaks, θ is Bragg angle and λ=1.54Å is the wavelength of Cu Kα radiation. The calculated crystalline size and lattice parameters are 26.87, 24.57, 25.17, 25.63 and 0.6128, 0.624, 0.6086, 0.6004 for x=0, 0.05, 0.10, 0.15 respectively. As the nickel content increases, crystalline nature and crystalline size also increase. But the lattice constant decreases due to changes in bond length. This may be attributed to the replacing of some of Pb^{2+} ions with Ni^{2+} ions since the ionic radius of Ni^{2+} (0.69 Å) is smaller than that of Pb^{2+} (1.19 Å). For precipitation process, ionic product constant (Q_{sp}) is greater than or equal to the solubility product constant (K_{sp}).

3.2. SEM and EDAX analysis

The SEM micrographs of $Pb_{1-x}Ni_xSe$ (x= 0, 0.05, 0.10, 0.15) samples are shown in Fig. 2 (a-d). For increasing dopant content, SEM micrograph shows a well defined structure in crystalline nature and it is a good agreement to XRD. Some fine and coarse cubical structure with aggregate is noticed. The average particle size is calculated using line section method from SEM micrographs in the range of 35-55 nm. It is evident that the particle size increases significantly with the nickel content and structure being changed from coarse amorphous to

crystalline particles. This may be due to increase of Ni^{2+} ions in host matrices which accelerate the growth of grain size. Further, it is reported that the cubic symmetry of PbSe grows without constraint; it prefers to grow in cubic shape [20, 21].
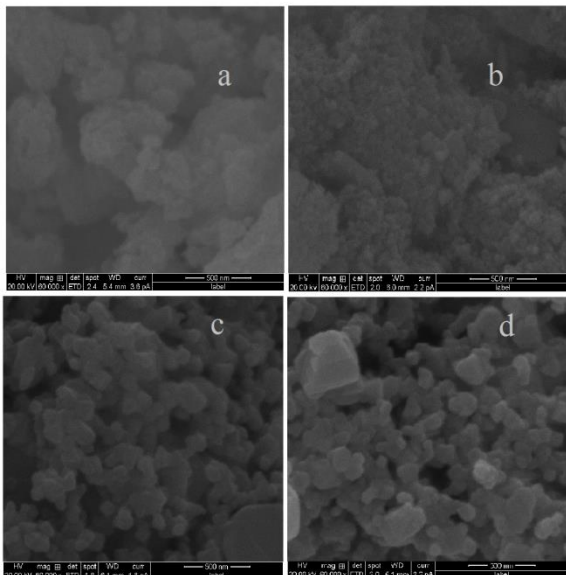
Fig. 2(a-d) SEM micrograph of $Pb_{1-x}Ni_xSe$ (X=0, 0.05, 0.10, 0.15) nanoparticles at pH 9.0
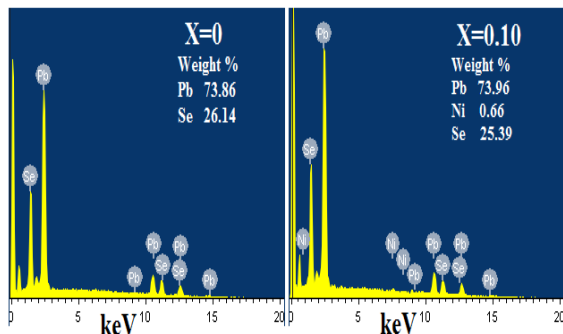
Fig. 3. EDX spectra of pure and 0.10 M nickel doped PbSe nanoparticles

Compositional analysis of the samples is done through EDAX investigations and the presence of Pb, Ni, Se is confirmed as shown in Fig 3. All the samples show stoichiometry weight percentage without any impurities. The atomic weight percentages are in good agreement with the composition.

3.3. TEM analysis

The TEM micrographs and selected area electron diffraction pattern (SAED) of samples with x=0 and x=0.10 ($Pb_{1-x}Ni_xSe$) are shown in Fig. 4 (a-d). The particles are found to be spherical in shape and it is close

to the size calculated from Scherer's equation. The SAED pattern confirms the crystalline nature of the samples and the sample with x=0. 10 has high crystalline nature with a cubic crystal structure. For x=0, the particles seem to agglomerate each other, but the agglomeration reduces for x=0.10 and in certain regions, dark areas are noticed due to a congregation of nano particles. This occurs due to high surface energy, dipole interaction and large specific surface area of transition metal doped nanoparticles [22].
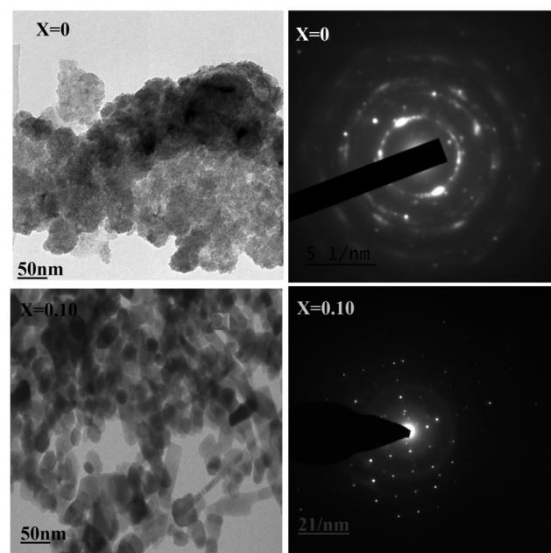
Fig. 4. TEM and SAED pattern of $Pb_{1-x}Ni_xSe$ (X=0 and 0.10) nanoparticles

3.4. Optical analysis

The optical absorption of $Pb_{1-x}Ni_xSe$ (x= 0, 0.05, 0.10, 0.15) nanoparticles were measured in the range from 300-2000 nm. The absorption spectrum, as shown in Fig. 5 indicates the presence of absorbance peaks in the visible region and Near Infra-Red (NIR) region.
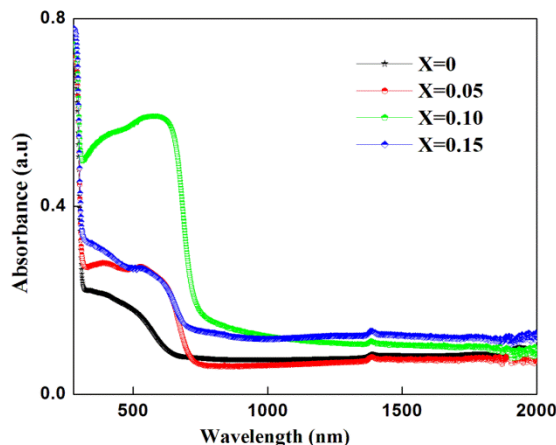
Fig. 5. UV-Visible absorption spectra of $Pb_{1-x}Ni_xSe$ (X=0, 0.05, 0.10, 0.15) nanoparticles

Broad peak centered on 600 nm can be observed in all samples and this shows a considerable blue shift because of the strong confinement of nanoparticles. This may attribute to the excitonic effect due to carrier confinement produced through correlation between confined electrons and holes [23]. The broad absorption peak reveals the transition in quantum regime, which may due to inhomogeneous broadening effect [24]. Absorption is found to increase with nickel content and decrease for x=0.15. The band structure and optical band gap value E_g can be obtained from the absorption spectrum. In crystalline material, at absorption edge, the electronic transition is found between the lowest energy of the conduction band and the highest energy of the valence band. The fundamental absorption edge in most chalcogenide follows an exponential law and it obey following relation [25],

$$(\propto h\nu)^{1/n} = B(h\nu - E_g) \tag{2}$$

Where α can be derived from the absorption spectrum according to Lambert-Beer equation applied to powder [24], h is the Planck's constant, ν is the incident beam frequency, B is a constant and n is an exponent, which has the values of 1/2, 3/2, 2 and 3 depending on the nature of the electronic transition. The electronic transition of $Pb_{1-x}Ni_xSe$ chalcogenides obeys the direct transition, indicating n=1/2. The evaluated values of band gap energies are 1.92, 1.82, 1.71, 1.68 eV for the samples of $Pb_{1-x}Ni_xSe$ (X=0, 0.05, 0.10, 0.15) respectively are shown in Fig. 6.
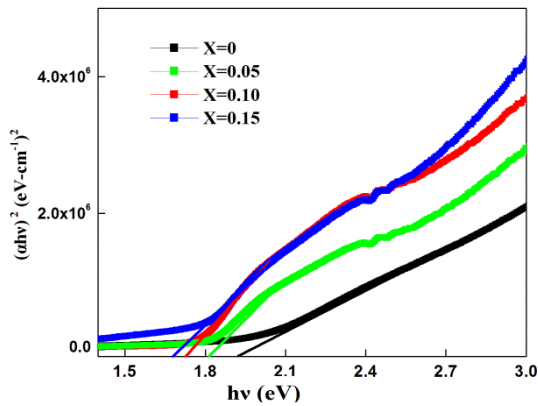
Fig. 6. $(\alpha h\nu)^2$ against photon energy (hν) in $Pb_{1-x}Ni_xSe$ (X=0, 0.05, 0.10, 0.15) nanoparticles

The band gap value decreases with increase of nickel content and this may due to increase in crystallinity. According to previous reports, hydrazine hydrate also plays a major role for reduction in band gap [26].

3.5. Dielectric analysis

The value of dielectric constant was calculated using the relation:

$$\varepsilon` = \frac{d \, C_p}{A \, \varepsilon_0} \tag{3}$$

Where, ε_0 is the free space permittivity and equal to 8.854×10^{-12} F/m, d is pellet thickness, A is the cross sectional area of the flat surface of the pellet ad C_p is the capacitance of the sample in Farad (F).
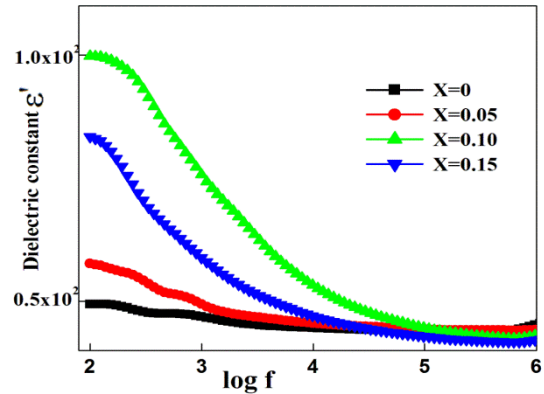
Fig. 7. Dielectric constant of $Pb_{1-x}Ni_xSe$ (X=0, 0.05, 0.10, 0.15) nanoparticles

Fig. 7 illustrates the variation of dielectric constant with the logarithm of frequency ranging from 100 Hz to 5 MHz for $Pb_{1-x}Ni_xSe$ (X=0, 0.05, 0.10, 0.15) samples. The dielectric constant value of all samples decreases with increase in frequency and becomes constant at higher frequency. The dielectric constant decreases rapidly in low frequency and slow in high frequency, this behavior can explain on the basis of Koop`s theory and Maxwell-Wagner two layer model [27,28]. According to this model, a system containing dielectric materials has highly conducting grains separated by highly thin resistive grain boundaries. The higher values of dielectric constant at low frequency are due to interfacial space charge polarization. In the presence of external field, the dipole moment formed due to the combination of random positive and negative ions and these ions align themselves in the direction of field inducing rotation dielectric polarization (RDP). And also, space charge will move in the opposite direction to the field and get trapped by the defects present in the nanocrystalline materials and this induces the space charge polarization (SCP) to enhance ε` values and keep the grain boundary electrically active. The dielectric constant decreases with frequency and increases with nickel content, which is closely in agreement with Debye relaxation mode for orientation polarization [29]. Due to Ni doping crystallinity increase, this also results in the enhancement of RDP and SCP.

4. Conclusion

In summary, $Pb_{1-x}Ni_xSe$ (x= 0, 0.05, 0.10, 0.15) nanoparticles consisting of coarse nanocube texture with preferred orientation were successfully synthesized at room temperature via simple wet chemical route. The

XRD spectra show average crystallite size in the range of 24-26 nm with face-centered cubic structure. As dopant concentration increases, particle size increases; whereas the lattice constant and interplanar spacing decreases due to substitution of smaller Ni^{2+} ion in host lattice. SEM micrographs show amorphous powder for pure lead selenide and well defined particles for increasing dopant concentration. The TEM micrographs confirm the crystalline nature and particle size. The absorption spectrum exhibits a prime absorption around 600nm and the band gap value decreases with increase of nickel content. The optical observation shows a considerable blue shift and confirms the strong confinement of nanoparticles. The dielectric constant value decreases with increase in frequency and increase with nickel. Hence, this method has potential application for large scale synthesis, high yield product and simple reaction mechanism which can be carried out for other metal chalcogenides.

References

[1] W. R. Feng, H. Zhou, F. Chen, Vacuum **114**, 82 (2015).

[2] P. A. Loiko, G. E. Rachkovskaya, G. B. Zacharevich, V. S. Gurin, M. S. Gaponenko, K. V. Yumashev, J. Non-Cryst. Solids **358**, 1840 (2012).

[3] K. F. Cai, X. R. He, Mater. Lett. **60**, 2461 (2006).

[4] F. J. Meca, M. M. Quintas, F. J. R. Sanchez, Sens. Actuator **84**, 45 (2000).

[5] M. F. Kotkata, M. S. Al-Kotb, I. G. El-Houssieny, Phys. Sci. **89**, 115805 (2014).

[6] T. Tohidi, K. Jamshidi-Ghaleh, Appl. Phys. A **118**, 1247 (2015).

[7] V. Arivazhagan, M. M. Parvathi, S. Rajesh, Vacuum **99**, 95 (2014).

[8] Xigui Sun, Kewei Gao, Xiaolu Pang, Huisheng Yang, Alex A Volinsky, Thin Solid Films **592**, 59 (2015).

[9] D. Rached, M. Rabah, N. Benkhettou, M. Driz, B. Soudini, Phys. B **337**, 394 (2003).

[10] F. J. Meca, M. M. Quintas, F. J. R. Sanchez, Sens. Actuator **84**, 45 (2000).

[11] Miloslav Frumar, Tomas Wagner, Curr. Opin. Solid State Mater. Sci. **7**, 117 (2003).

[12] T. Ding, H. Wang, S. Xu, J. J. Zhu, J. Cryst. Growth **235**, 517 (2002).

[13] H. Tong, Y. J. Zhu, L. X. Yang, L. Li, L. Zhang, Angew. Chem. Int. Ed. **45**, 7739 (2006).

[14] U. K. Gautam, R. Seshadri, Mater. Res. Bull. **39**, 669 (2004).

[15] W. X. Zhang, L. Zhang, Y. W. Cheng, Z. H. Hui, X. M. Zhang, Y. Xie, Y. T. Qian, Mater. Res. Bull. **35**, 2009 (2000).

[16] Shamshad A. Khan, Zishan H. Khan, A. A. El-Sebaii, F. M. Al-Marzouki, A. A. Al-Ghamdi, Physica B **405**, 3384 (2010).

[17] J. J. Zhu, Y. Koltypin, A. Gedanken, Chem Mater. **12**, 73 (2000).

[18] Wenran Feng, Hai Zhou, Fei Chen, Vacuum **114**, 82 (2015).

[19] E. L. Kadry, A. Ashour, S. A. Mahmoud, Thin Solid Films **269**, 112 (1995).

[20] M. Hatami, M. H. Majles Ara, A. Rostami, M. Dolatyari, M. Mahmudi, H. Baghban, H. Rasooli, M. Afsare, Int. J. Nanosci. Nanotechnol. **83**, 149 (2012).

[21] Alireza Khataee, Samira Arefi-Oskoui, Mehrangiz Fathinia, Arezoo Fazli, Ali Shahedi Hojaghan, Younes Hanifehpour, Sang Woo Joo, J. Industrial and Engineering Chemistry **30**, 134 (2015).

[22] R. B. Kale, S. D. Sartale, V. Ganesan, C. D. Lokhande, Yi-Feng Lin, Shih-Yuan Lu, Appl. Surf. Sci. **253**, 930 (2006).

[23] Masoud Salavati-Niasari, Bahareh Shoshtari-Yeganeh, Mehdi Bazarganipour, Superlattices and Microstructures **58**, 20 (2013).

[24] Y. Liu, J. Cao, J. Zeng, C. Li, Y. Qian, S. Zhang, Eur. J. Inorg. Chem. **2003**, 644 (2003).

[25] A. A. Al-Ghamdi, S. Al-Heniti, Shamshad A. Khan, J. Lumin. **135**, 295 (2013).

[26] K. C. Preetha, T. L. Remadevi, Materials Science in Semiconductor Processing **39**, 178 (2015).

[27] C. G. Koops, Phys. Rev. **83**, 121 (1951).

[28] J. C. Maxwell, A Treaties on Electricity and Magnetism Clarendon, Oxford (1892).

[29] H. Birey, J. Appl. Phys. **49**, 2898 (1978).

_____
*Corresponding author: prsr72@gmail.com